Few-Atom-Thick Colloidal PbS/CdS Core/Shell Nanosheets

Simeen Khan,[†,‡] Zhoufeng Jiang,[§,†,‡] Shashini M. Premathilka,[§,†] Antara Antu,[†] Jianjun Hu,[#] Andrey A. Voevodin,[#,⊥] Paul J. Roland,[¶] Randy J. Ellingson,[¶] and Liangfeng Sun[*,§,†]

[†]Department of Physics and Astronomy, Bowling Green State University, Bowling Green, Ohio 43403, United States

[§]Center of Photochemical Sciences, Bowling Green State University, Bowling Green, Ohio 43403, United States

[#]Materials and Manufacturing Directorate, Air Force Research Laboratory, Wright-Patterson Air Force Base, Ohio 45433, United States

[¶]Department of Physics and Astronomy, Wright Center for Photovoltaics Innovation and Commercialization, School of Solar and Advanced Renewable Energy, University of Toledo, Toledo, Ohio 43606, United States

Ⓢ *Supporting Information*

ABSTRACT: Emissive PbS/CdS core/shell nanosheets are synthesized using a cation-exchange method. A significant blue-shift of the photoluminescence is observed, indicating a stronger quantum confinement in the PbS core as its thickness is reduced. High resolution transmission-electron-microscopy images of the cross sections of the core/shell nanosheets show atomically sharp interfaces between PbS and CdS. Accurate analysis of the thickness of each layer reveals the relationship between the energy gap and the thickness in the extremely one-dimensionally confined nanostructure. Photoluminescence lifetime of the core/shell nanosheets is significantly longer than the core-only nanosheets, indicating better surface passivation.
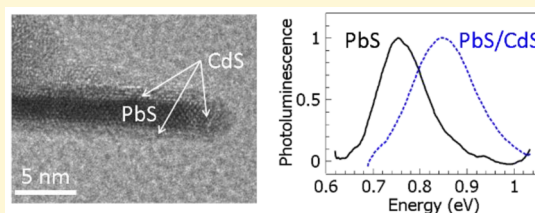
Quantum confinement is the origin of the novel properties of quantum dots. However, three-dimensional confinement also hinders the charge transfer among the quantum dots, which limits the performance of the quantum-dot-based electronic devices. In a two-dimensional (2D) structure, the charges within the 2D plane have high charge mobilities[1,2] while the one-dimensional quantum confinement is retained in the thickness direction. Consequently, the tunable optical properties and the high charge mobility are unified in a single structure. Among the artificial 2D materials, IV−VI nanosheets are particularly interesting. Due to the large exciton Bohr radii in lead salts, strong quantum confinement can be easily achieved.[3] The small energy gaps of the IV−VI semiconductors are also optimal to exploit carrier multiplication in solar cells. As recently demonstrated in colloidal PbS nanosheets,[4] 2D structures of these materials can increase carrier multiplication efficiency which correlates with the enhanced electron−hole Coulomb interaction[5] in the anisotropic structure. In addition, the spin−orbital coupling is strong in IV−VI materials.[6,7] When it interplays with quantum confinement in the 2D structure, a new class of material, topological crystalline insulators, can be created.[8] These materials have surface states that exhibit linear dispersion with a single Dirac cone, and charge transfer in the surface states is protected against backscattering by crystal symmetry.[9−11] These surface states can be more easily observed in 2D structures due to their large surface-to-volume ratio.[12−16] These novel properties are critical for low-dissipation devices, superconductors, and quantum computers.[17,18] So far, theoretical work has predicted that a series of 2D IV−VI materials

including SnTe,[9,19] PbS,[9−11] PbSe,[8,9] and PbTe[9,19] can be turned into topological crystalline insulators through tuning the thickness,[9] exerting a strain,[11] or applying an electric field.[10]

These properties are mainly determined by size (quantum confinement), shape (anisotropy of spatial and dielectric confinement), and crystal heterostructures (strain). Creation of thickness tunable core/shell 2D nanosheets can partially address the challenges. A wet-chemistry synthesis of colloidal nanosheets[1,20−26] followed by cation exchange will create such structures. The synthesized colloidal nanosheets are counterparts of the epitaxial quantum wells[27] but are free-standing and have low-cost (since no high-vacuum or high-temperature is needed for the synthesis).[28] In this Article, we report a facile synthesis of emissive PbS/CdS core/shell nanosheets with emphasis on the energy-gap tunability. We demonstrate that the energy gap of the PbS core can be systematically tuned from 0.75 to 0.93 eV through changing the reaction conditions. The tunable energy gap, while combined with the strong spin−orbit interaction in PbS, provides an opportunity to tune the topological property of the material.[8] High resolution transmission electron microscopy (HRTEM) images of the cross-section of the nanosheets show clear crystal interfaces between PbS and CdS. It also provides an alternative method that can precisely determine the thicknesses of the PbS core and the CdS shell of the 2D heterostructure as well as the pure PbS nanosheets, while avoiding the effect of capping ligands or the

fitting errors in the thickness determination using atomic-force microscopy[4,29] or X-ray diffraction.[4,21] It will help to resolve a debated problem, the energy gap dependence on the thickness of the nanosheets, which is partially due to the difficulty in measuring the thickness accurately.[4,21,29] Photoluminescence lifetime of core/shell nanosheets is significantly longer than the core-only nanosheets, indicating a better surface passivation. The core/shell structures with improved surface properties are important for further multiple-exciton-generation study. The strain introduced at the interface of PbS and CdS alters the electronic structure of PbS and may create a topological crystalline insulator as theoretically predicted.

The synthesis of PbS nanosheets (Supporting Information A) is based on the methods invented by Weller's group[21] and developed by others.[1,29] After PbS nanosheets are synthesized and purified, a cation-exchange method[30,31] is used to exchange the outer layer Pb ions with Cd ions to form a CdS shell surrounding the PbS core. In brief, cadmium oxide is mixed with oleic acid and heated under nitrogen to form cadmium oleate, which is then mixed with PbS nanosheets for the cation-exchange reaction. The reaction is stopped by adding cold hexane. The final solution is washed twice with toluene and finally dispersed in toluene (Supporting Information A). This method does not change the overall thickness of the nanosheets but rather reduces the thickness of PbS core (Figure 1a).
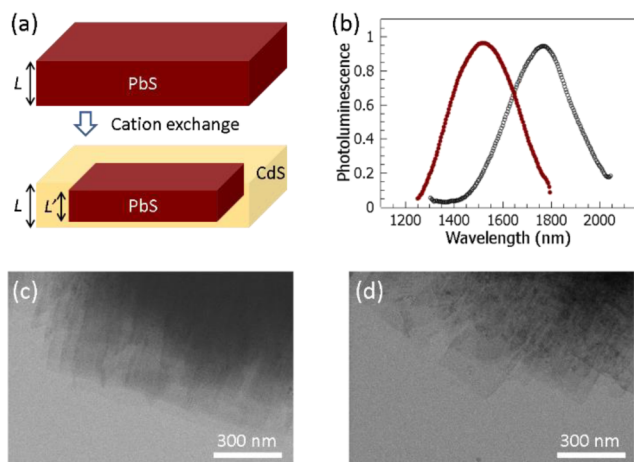
Figure 1. (a) Scheme showing the process of cation exchange for the PbS/CdS structure. The overall dimension of the sheet remains the same while the out-layers of the material turn into CdS. (b) Photoluminescence spectra from the nanosheets before (open circles) and after (solid circles) cation exchange showing the shift of the peak from 1760 to 1520 nm. (c) TEM image of the stacked original PbS nanosheets. Each nanosheet has a lateral size of a few hundred nanometers. (d) TEM image of the stacked nanosheets after cation exchange showing a similar morphology as in (c).

The transmission electron microscopy (TEM) images (Figure 1c,d) and secondary-electron images (Supporting Information B) show that the morphology of the nanosheets remains the same after cation exchange. However, there is a significant blue-shift (Figure 1b) of the photoluminescence (Supporting Information C), indicating the decrease of the thickness of the PbS core. Further energy-dispersive X-ray spectroscopy measurements show a clear Cd peak after cation exchanges (Supporting Information D).

To learn the details of the heterostructure formed in PbS/CdS nanosheets, it is essential to prepare the nanosheets

standing on edge so that the cross sections of the nanosheets can be imaged using HRTEM. To achieve this goal, small-lateral-size nanosheets having a width of around 20 nm are synthesized using a modified procedure (Supporting Information A). The narrow width of the nanosheet makes it easy for them to stand up on the TEM substrate (Figure 2a). The
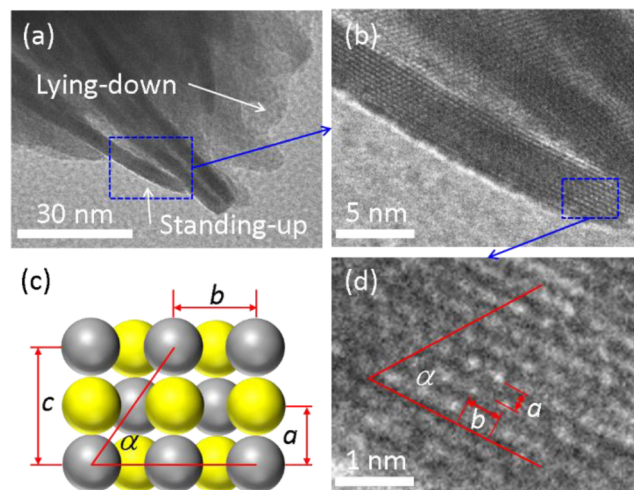
Figure 2. (a) TEM image of PbS nanosheets showing both standing-up and lying-down nanosheets. (b) The HRTEM image of one standing-up nanosheet shows a single-crystalline structure with 12 layers of atoms in the thickness direction. (c) Diagram showing the arrangement of the atoms viewed in the ⟨110⟩ direction of the crystal. (d) In the thickness direction, the spacing between the neighbor atoms a is 0.297 nm, while in the orthogonal direction, the spacing between the neighbor atoms b is 0.42 nm. The angle α is about 55°.

HRTEM image (Figure 2b) shows an array of dots which is the projection of the atoms in the nanosheets onto the substrate. This image reveals that the surfaces of the nanosheets are nearly atomically flat. The standing-up PbS nanosheets show a single-crystal structure with 12 atomic layers in the thickness direction. The thickness can be calculated by multiplying the lattice constant of PbS ($c = 0.594$ nm) by the multiple of lattice constant the thickness spans (5.5), resulting in a thickness determination in this case of 3.27 nm. This thickness matches that obtained (3.3 ± 0.1 nm) using the calibrated HRTEM instrument (Supporting Information E). The dependence of the energy gap on the thickness of the PbS nanosheets is still under debate,[4,21,29] partially due to the difficulty of the thickness measurements. Since the nanosheets can be prepared standing-up on the substrate, their thickness can be accurately measured without ambiguity.

All of the observed cross sections of the nanosheets show the same facet as in Figure 2b. For the projection of {110} facet of PbS crystal (Figure 2d), the spacing between neighbor atoms in the ⟨001⟩ direction is $a = c/2 = 0.297$ nm, while the spacing between the neighbor atoms (within the same plane) in the orthogonal direction ⟨110⟩ is $b = c/\sqrt{2} = 0.420$ nm. The angle α (Figure 2d) between the line of the same atoms and ⟨110⟩ direction is then 55° (Supporting Information F). All of the parameters a, b, and α as measured using HRTEM (Figure 2c) match up with the calculated results above. This confirms the observed surface of the nanosheet edge has a {110} facet and the top/bottom surfaces of the nanosheet have a {001} facet. This result is consistent with the earlier 2D oriented attachment model[21] for the growth mechanism of 2D PbS nanosheets; i.e.,

the PbS quantum dots attach to each other through {110} facets, resulting in {110} facets at the edges of the nanosheets.

The same PbS nanosheets are used to synthesize PbS/CdS core/shell nanosheets. After cation exchange, the core/shell nanosheet shows atomically sharp interfaces between PbS and CdS (Figure 3). The PbS core has about 8 atomic layers,
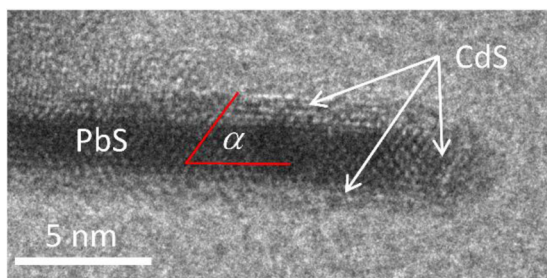
Figure 3. HRTEM image showing sharp interfaces between the PbS core and the CdS shell. The crystal structure of the CdS shell is similar to the PbS core. The lines are to guide the eyes to the array of atoms, making an angle α unique to the {110} facet.

indicating ~2 atomic layers of PbS have been turned into CdS on each side of the nanosheet, reducing the thickness of the PbS core to 2.1 nm as measured with HRTEM (Supporting Information E). The HRTEM image (Figure 3) of the cross-section of the PbS/CdS nanosheet shows a {110} facet as in the original PbS nanosheet (Figure 2c). At some locations, the crystal structure of the CdS shell remains nearly the same as the PbS core as in the case of core/shell PbS/CdS quantum dots,[32] while it appears amorphous at other locations (Figure 3). The PbS/CdS heterostructure is clearly revealed by the sharp contrast in the HRTEM image, which is due to the high atomic-weight ratio Pb/Cd.

At the {100} facets (top/bottom surfaces) of the PbS nanosheet, the interfaces between PbS and CdS are nearly atomically flat, indicating that the cation exchange occurs uniformly from the surface into the bulk of the nanosheet. This differs from what was observed in PbSe/CdSe nanorods,[33] for which a zigzag-shaped core terminated by {111} interfaces formed. The reaction temperature is believed to play a key role in achieving uniform cation exchange. On the other hand, smaller surface to volume ratios in 2D sheets in contrast to 1D nanorods likely favor a uniform cation-exchange. Similar work by Dubertret and co-workers demonstrated that flat interfaces formed after cation-exchanges in PbSe/PbS, CdSe/CdS, and ZnSe/ZnS nanoplatelet.[34] At the {110} facets (edge surfaces) of the PbS nanosheet, the CdS shells are significantly thicker than the shells at {100} facets and the PbS/CdS interface is less sharp (Figure 3), which is likely due to the high reactivity of the {110} facets.[21]

The element mapping of the vertically aligned PbS/CdS core/shell nanosheets shows the same image for Pb, Cd, and S elements, and each of them overlaps with the high-angle-annular-dark-field image (Supporting Information G). It reveals that the cation exchange occurs nonselectively. At this time, the resolution of the element mapping is not high enough to map out the elements layer by layer, but the element analysis over the ensemble of the nanosheets shows the molar ratio of lead (Pb) to cadmium (Cd) is around 2.4:1 (Supporting Information G). It is consistent with the HRTEM analysis: around 8 layers of PbS versus 4 layers of CdS.

The PbS/CdS nanosheets fluoresce in the infrared as the original PbS nanosheets,[29] in contrast to nonemissive ZnSe/ZnS and PbSe/PbS core/shell nanoplatelets.[34] Those nanoplatelets were created using two-step cation-exchange: CdSe/CdS to Cu_2Se/Cu_2S and then to ZnSe/ZnS or PbSe/PbS. The excess trap sites formed by the residue copper atoms were thought to quench the photoluminescence.[34] Our emissive nanosheets help to determine the optical energy gap, since the Stokes' shift is negligible for PbS nanosheets[29] as well as for PbS/CdS nanosheets (Supporting Information H). The photoluminescence of the core/shell nanosheets shows a significant blue-shift as compared with the original PbS nanosheets (Figure 4a), indicating stronger quantum confine-
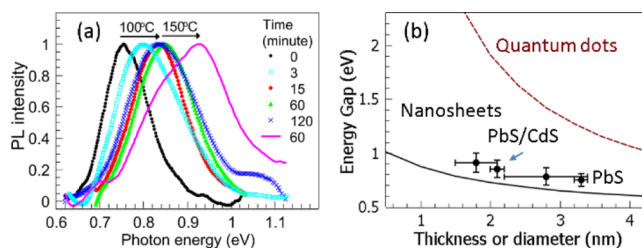
Figure 4. (a) The photoluminescence peak shifts from 0.75 to 0.80 eV after cation exchange for 3 min at 100 °C. It shifts to 0.83 eV after 15 min. After that, longer reaction times (60 and 120 min) do not shift the peak more but stabilize it between 0.84 and 0.85 eV. Further increase of the reaction temperature to 150 °C shifts the peak to 0.93 eV after an additional 60 min cation exchange. (b) Comparison of the energy-gap of the nanosheets (solid dots), the nanosheet model developed earlier (solid line)[29] and PbS quantum dots (dashed line).[35] The arrow indicates the data from PbS/CdS core/shell nanosheets obtained through cation exchange from the 3.3 nm thick PbS nanosheets (the rightmost dot).

ment due to the decrease of the core thickness after cation exchange. At 100 °C reaction temperature, the photoluminescence shift mainly occurs within 15 min after reaction. The shift is small beyond 15 min, indicating that the cation-exchange process is self-limiting at a certain reaction temperature (Figure 4a). However, increase of the reaction temperature can further the cation exchange, resulting in more blue-shift of the photoluminescence peak (Figure 4a). So far, we have achieved tunability of the photoluminescence peak in PbS/CdS core/shell nanosheets from 0.75 to 0.93 eV, corresponding to the wavelength range from 1333 to 1653 nm. For the small-lateral-size PbS nanosheets, the optical energy gaps obtained from photoluminescence spectroscopy and the thicknesses obtained using HRTEM are plotted together in Figure 4b. The data points are slightly above the fitting curve obtained previously.[29] The slightly larger energy gap is likely due to the additional confinement in the width direction since the width of the nanosheets is about 20 nm which is close to the exciton Bohr radius of PbS. After cation exchange, the decrease of the PbS thickness results in a larger energy gap. The relationship between the energy gap and the thickness is consistent with these obtained from core-only PbS nanosheets (Figure 4b). As expected, the confinement energy in either the PbS nanosheets or PbS/CdS core/shell nanosheets is much less than in quantum-dots with the diameter equal to the thickness of the nanosheets. This is mainly due to the difference of 3D confinement (QDs) and 1D confinement (nanosheets).[29]

The average thickness of the PbS core (so is the CdS shell) can be precisely tuned by the reaction conditions. The accuracy of the thickness, as can be derived from the photoluminescence peak (Figure 4), reaches a subnanometer level.

At a higher reaction temperature (150 °C), thinner (2.1 nm) PbS nanosheets can be nearly completely turned into CdS nanosheets. The photoluminescence peak around 1540 nm corresponding to the original PbS nanosheets disappears completely but a peak at 430 nm appears. Energy-dispersive X-ray spectroscopy confirms the amount of Pb in the product is negligible (Supporting Information I).

Creation of the core/shell structure also increases the lifetime of the photoluminescence (Supporting Information J) from the PbS core. The decay of the photoluminescence intensity from the nanosheets is not single-exponential. The $1/e$ photoluminescence intensity occurs at 4 and 7 ns for PbS nanosheets and PbS/CdS nanosheets, respectively (Figure 5). The nearly
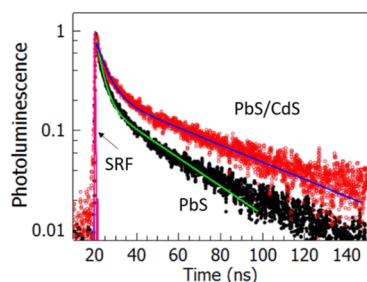
Figure 5. Photoluminescence lifetimes of the PbS (solid circles) and PbS/CdS (open circles) nanosheets. Each lifetime is measured at the peak intensity of the photoluminescence, 0.75 eV for PbS nanosheets and 0.83 eV for PbS/CdS nanosheets. The solid lines passing through the data points are the fitting curves. The system response function (SRF) is also shown.

doubled decay time in the core/shell nanosheets is likely due to a better surface passivation of the PbS core after cation exchange, instead of type II heterostructure (Supporting Information K). It is consistent with the improved photoluminescence intensity (normalized to absorption) from the core/shell nanosheets (Supporting Information L). Aging of the PbS nanosheets in toluene was demonstrated recently to improve the photoluminescence efficiency by an order of magnitude.[36] The mechanism in this experiment is different, but both methods have significantly improved the optical properties of the nanosheets. The photoluminescence decay can be fitted well using double exponential functions, yielding a fast decay of 2.9 ns (core only) and 4.9 ns (core/shell) and a slow decay of 30 ns (core only) and 51 ns (core/shell). The nature of the double-exponential decay of the photoluminescence intensity is still under investigation. In contrast to PbS quantum dots, PbS nanosheets and their core/shell structures have much shorter photoluminescence lifetimes. It is likely that the reduced dielectric screening in the 2D structure shortens the lifetime, as demonstrated by Ithurria and co-workers on CdSe nanoplatelets.[26] Surface defects can also shorten the photoluminescence lifetime by creating non-radiative decay channels. However, their effect can be reduced by surface-passivation methods, among which creating a CdS shell on the PbS core is an effective one, as demonstrated above.

It has been demonstrated that the strain between the PbS core and the CdS shell exists in PbS/CdS core/shell

nanocrystals.[32] It is expected that the strain also exists in PbS/CdS core/shell nanosheets, which will alter the electronic structure of the core, providing an additional parameter to tune the topological properties of the nanosheets.[37] However, the strain effect is only significant at the PbS layers which are close to the PbS/CdS interface. We expect to see the effect when the PbS core has only one to two atomic layers. The range of the thickness tunability shown earlier has not yet reached that region, so the electronic structure of PbS is still mainly determined by the thickness.

In summary, a facile synthesis of PbS/CdS core/shell nanosheets is developed. The core/shell heterostructure synthesized using cation-exchange methods has an increased energy gap and a longer photoluminescence lifetime. Proper preparations of standing-up nanosheets enable accurate characterizations of the core/shell crystal structures as well as their thicknesses. The HRTEM reveals that the interface between PbS and CdS is nearly atomically flat. It is expected that this method can be used to create thinner (less than 8 atomic layers) PbS sheets capped by CdS using thinner original PbS nanosheets and/or adjusting the reaction conditions. In these extremely thin core/shell nanosheets, novel electronic properties (e.g., topological properties) may occur as theoretically predicted. On the other hand, the improved optical properties are also important for further studies on the exciton dynamics in the 2D materials.

■ ASSOCIATED CONTENT

Ⓢ Supporting Information

The Supporting Information is available free of charge on the ACS Publications website at DOI: 10.1021/acs.chemmater.6b01232.

Synthesis procedures for PbS nanosheets and PbS/CdS core/shell nanosheets; secondary-electron microscopy images of nanosheets; photoluminescence measurements; energy-dispersive X-ray spectroscopy; thickness measurements; geometry of the {110} facet of PbS; STEM and element mapping; Stokes' shift; complete transformation of PbS nanosheets; photoluminescence lifetime measurements (PDF)

■ AUTHOR INFORMATION

Corresponding Author
*E-mail: lsun@bgsu.edu.

Present Address
⊥A.A.V.: Department of Materials Science and Engineering, College of Engineering, University of North Texas, Denton, Texas 76203, United States.

Author Contributions
‡S.K. and Z.J. contributed equally.

Notes
The authors declare no competing financial interest.

■ ACKNOWLEDGMENTS

■ ABBREVIATIONS

HRTEM, high resolution transmission electron microscopy; TEM, transmission electron microscopy; 2D, two-dimensional

■ REFERENCES

(1) Dogan, S.; Bielewicz, T.; Cai, Y.; Klinke, C. Field−effect transistors made of individual colloidal PbS nanosheets. *Appl. Phys. Lett.* **2012**, *101*, 073102.

(2) Dogan, S.; Bielewicz, T.; Lebedeva, V.; Klinke, C. Photovoltaic effect in individual asymmetrically contacted lead sulfide nanosheets. *Nanoscale* **2015**, *7*, 4875−4883.

(3) Machol, J. L.; Wise, F. W.; Patel, R.; Tanner, D. B. Optical studies of IV−VI quantum dots. *Phys. A* **1994**, *207*, 427−434.

(4) Aerts, M.; Bielewicz, T.; Klinke, C.; Grozema, F. C.; Houtepen, A. J.; Schins, J. M.; Siebbeles, L. D. A. Highly efficient carrier multiplication in PbS nanosheets. *Nat. Commun.* **2014**, *5*, 3789.

(5) Yang, J.; Hyun, B. R.; Basile, A. J.; Wise, F. W. Exciton relaxation in PbSe nanorods. *ACS Nano* **2012**, *6*, 8120−8127.

(6) Okoye, C. Electronic and optical properties of SnTe and GeTe. *J. Phys.: Condens. Matter* **2002**, *14*, 8625−8637.

(7) Dyrdal, A.; Dugaev, V. K.; Barnas, J. Spin Hall effect in IV-VI semiconductors. *Epl* **2009**, *85*, 67004.

(8) Wrasse, E. O.; Schmidt, T. M. Prediction of Two-Dimensional Topological Crystalline Insulator in PbSe Monolayer. *Nano Lett.* **2014**, *14*, 5717−5720.

(9) Liu, J.; Qian, X.; Fu, L. Crystal Field Effect Induced Topological Crystalline Insulators In Monolayer IV−VI Semiconductors. *Nano Lett.* **2015**, *15*, 2657−2661.

(10) Liu, J.; Hsieh, T. H.; Wei, P.; Duan, W.; Moodera, J.; Fu, L. Spin-filtered edge states with an electrically tunable gap in a two-dimensional topological crystalline insulator. *Nat. Mater.* **2014**, *13*, 178−183.

(11) Hsieh, T. H.; Lin, H.; Liu, J.; Duan, W.; Bansil, A.; Fu, L. Topological crystalline insulators in the SnTe material class. *Nat. Commun.* **2012**, *3*, 982.

(12) Cha, J. J.; Koski, K. J.; Cui, Y. Topological insulator nanostructures. *Phys. Status Solidi RRL* **2013**, *7*, 15−25.

(13) Hong, S. S.; Cha, J. J.; Kong, D.; Cui, Y. Ultra-low carrier concentration and surface-dominant transport in antimony-doped Bi2Se3 topological insulator nanoribbons. *Nat. Commun.* **2012**, *3*, 757.

(14) Peng, H.; Lai, K.; Kong, D.; Meister, S.; Chen, Y.; Qi, X.; Zhang, S.; Shen, Z.; Cui, Y. Aharonov-Bohm interference in topological insulator nanoribbons. *Nat. Mater.* **2010**, *9*, 225−229.

(15) Kong, D.; Randel, J. C.; Peng, H.; Cha, J. J.; Meister, S.; Lai, K.; Chen, Y.; Shen, Z.; Manoharan, H. C.; Cui, Y. Topological Insulator Nanowires and Nanoribbons. *Nano Lett.* **2010**, *10*, 329−333.

(16) Hong, S. S.; Kundhikanjana, W.; Cha, J. J.; Lai, K.; Kong, D.; Meister, S.; Kelly, M. A.; Shen, Z.; Cui, Y. Ultrathin Topological Insulator Bi2Se3 Nanoribbons Exfoliated by Atomic Force Microscopy. *Nano Lett.* **2010**, *10*, 3118−3122.

(17) Hasan, M. Z.; Kane, C. L. Colloquium: Topological insulators. *Rev. Mod. Phys.* **2010**, *82*, 3045−3067.

(18) Qi, X.; Zhang, S. Topological insulators and superconductors. *Rev. Mod. Phys.* **2011**, *83*, 1057−1110.

(19) Niu, C.; Buhl, P. M.; Bihlmayer, G.; Wortmann, D.; Blügel, S.; Mokrousov, Y. Topological crystalline insulator and quantum anomalous Hall states in IV-VI-based monolayers and their quantum wells. *Phys. Rev. B: Condens. Matter Mater. Phys.* **2015**, *91*, 201401.

(20) Acharya, S.; Sarma, D. D.; Golan, Y.; Sengupta, S.; Ariga, K. Shape-Dependent Confinement in Ultrasmall Zero-, One-, and Two-Dimensional PbS Nanostructures. *J. Am. Chem. Soc.* **2009**, *131*, 11282−11283.

(21) Schliehe, C.; Juarez, B. H.; Pelletier, M.; Jander, S.; Greshnykh, D.; Nagel, M.; Meyer, A.; Foerster, S.; Kornowski, A.; Klinke, C.; Weller, H. Ultrathin PbS sheets by two-dimensional oriented attachment. *Science* **2010**, *329*, 550−553.

(22) Acharya, S.; Das, B.; Thupakula, U.; Ariga, K.; Sarma, D. D.; Israelachvili, J.; Golan, Y. A Bottom-Up Approach toward Fabrication of Ultrathin PbS Sheets. *Nano Lett.* **2013**, *13*, 409−415.

(23) Joo, J.; Son, J. S.; Kwon, S. G.; Yu, J. H.; Hyeon, T. Low-Temperature Solution-Phase Synthesis of Quantum Well Structured CdSe Nanoribbons. *J. Am. Chem. Soc.* **2006**, *128*, 5632−5633.

(24) Ithurria, S.; Dubertret, B. Quasi 2D Colloidal CdSe Platelets with Thicknesses Controlled at the Atomic Level. *J. Am. Chem. Soc.* **2008**, *130*, 16504−16505.

(25) Son, J.; Wen, X.; Joo, J.; Chae, J.; Baek, S.; Park, K.; Kim, J.; An, K.; Yu, J.; Kwon, S.; Choi, S.; Wang, Z.; Kim, Y.; Kuk, Y.; Hoffmann, R.; Hyeon, T. Large-Scale Soft Colloidal Template Synthesis of 1.4? nm Thick CdSe Nanosheets. *Angew. Chem., Int. Ed.* **2009**, *48*, 6861−6864.

(26) Ithurria, S.; Tessier, M. D.; Mahler, B.; Lobo, R. P. S. M.; Dubertret, B.; Efros, A. L. Colloidal nanoplatelets with two-dimensional electronic structure. *Nat. Mater.* **2011**, *10*, 936−941.

(27) van der Ziel, J. P.; Dingle, R.; Miller, R. C.; Wiegmann, W.; Nordland, W. A. Laser oscillation from quantum states in very thin GaAs−Al0.2Ga0.8As multilayer structures. *Appl. Phys. Lett.* **1975**, *26*, 463−465.

(28) Yang, J.; Son, J. S.; Yu, J. H.; Joo, J.; Hyeon, T. Advances in the Colloidal Synthesis of Two-Dimensional Semiconductor Nanoribbons. *Chem. Mater.* **2013**, *25*, 1190−1198.

(29) Bhandari, G. B.; Subedi, K.; He, Y.; Jiang, Z.; Leopold, M.; Reilly, N.; Lu, H. P.; Zayak, A. T.; Sun, L. Thickness-Controlled Synthesis of Colloidal PbS Nanosheets and Their Thickness-Dependent Energy Gaps. *Chem. Mater.* **2014**, *26*, 5433−5436.

(30) Pietryga, J. M.; Werder, D. J.; Williams, D. J.; Casson, J. L.; Schaller, R. D.; Klimov, V. I.; Hollingsworth, J. A. Utilizing the Lability of Lead Selenide to Produce Heterostructured Nanocrystals with Bright, Stable Infrared Emission. *J. Am. Chem. Soc.* **2008**, *130*, 4879−4885.

(31) Moroz, P.; Liyanage, G.; Kholmicheva, N. N.; Yakunin, S.; Rijal, U.; Uprety, P.; Bastola, E.; Mellott, B.; Subedi, K.; Sun, L.; Kovalenko, M. V.; Zamkov, M. Infrared Emitting PbS Nanocrystal Solids through Matrix Encapsulation. *Chem. Mater.* **2014**, *26*, 4256−4264.

(32) Lechner, R. T.; Fritz-Popovski, G.; Yarema, M.; Heiss, W.; Hoell, A.; Schülli, T. U.; Primetzhofer, D.; Eibelhuber, M.; Paris, O. Crystal Phase Transitions in the Shell of PbS/CdS Core/Shell Nanocrystals Influences Photoluminescence Intensity. *Chem. Mater.* **2014**, *26*, 5914−5922.

(33) Casavola, M.; van Huis, M. A.; Bals, S.; Lambert, K.; Hens, Z.; Vanmaekelbergh, D. Anisotropic Cation Exchange in PbSe/CdSe Core/Shell Nanocrystals of Different Geometry. *Chem. Mater.* **2012**, *24*, 294−302.

(34) Bouet, C.; Laufer, D.; Mahler, B.; Nadal, B.; Heuclin, H.; Pedetti, S.; Patriarche, G.; Dubertret, B. Synthesis of Zinc and Lead Chalcogenide Core and Core/Shell Nanoplatelets Using Sequential Cation Exchange Reactions. *Chem. Mater.* **2014**, *26*, 3002−3008.

(35) Moreels, I.; Lambert, K.; Smeets, D.; De Muynck, D.; Nollet, T.; Martins, J. C.; Vanhaecke, F.; Vantomme, A.; Delerue, C.; Allan, G.; Hens, Z. Size-Dependent Optical Properties of Colloidal PbS Quantum Dots. *ACS Nano* **2009**, *3*, 3023−3030.

(36) Jiang, Z.; Bhandari, G. B.; Premathilaka, S. M.; Khan, S.; Dimick, D. M.; Stombaugh, C.; Mandell, A.; He, Y.; Peter Lu, H.; Sun, L. Growth of colloidal PbS nanosheets and the enhancement of their photoluminescence. *Phys. Chem. Chem. Phys.* **2015**, *17*, 23303−23307.

(37) Tang, E.; Fu, L. Strain-induced partially flat band, helical snake states and interface superconductivity in topological crystalline insulators. *Nat. Phys.* **2014**, *10*, 964−969.